The 2014 World Congress on
Advances in Civil, Environmental, and Materials Research (ACEM14)
Busan, Korea, August 24-28, 2014

Synthesis and Characterization of SnO_2 doped and un-doped In_2O_3 Nanoparticles for PV Application

* Saira Riaz[1)], Akram Raza and Shahzad Naseem[2)]

Centre of Excellence in Solid State Physics, University of the Punjab, Lahore, Pakistan
saira_cssp@yahoo.com

ABSTRACT

Tin oxide (SnO_2) doped and un-doped indium oxide (In_2O_3) nanoparticles are synthesized by the sol-gel method while anhydrous indium chloride ($InCl_3$) and anhydrous tin chloride ($SnCl_4$) are used as the source of indium and tin respectively, for the formation of indium tin oxide (ITO) thin films. Ethanol is used as solvent to get homogenous solution. Acetic acid (CH_3COOH) was also added drop wise in this solution. Thin films of doped and un-doped In_2O_3 are deposited on glass substrate at room temperature and annealed at different temperatures ranging from 50°C to 500°C. The XRD patterns of thin films indicates the main peak of $(12\bar{4})$ plane and showed a higher degree of crystallinity in annealed thin films. Average crystallite size of 10.9 nm to 29.3 nm is observed in all the deposited thin films. The optical transmittance spectra of SnO_2 doped In_2O_3 thin films showed the fundamental absorption edge with increment in annealing temperature. The band gap of thin films is observed to be from 3.35 eV to 3.57 eV which proves that these thin films have wide range of photovoltaic applications.

1. INTRODUCTION

Semiconductors with wide band gaps can be used as anti-reflecting coatings (AR) and front contacts or electrodes due to their transparency. ITO with wide band gap, high conductivity and low resistivity of 2 X 10^{-3} Ω can work as transparent electrical conductors. Tin-doped indium oxide (ITO) nanoparticles have a great significance in extensive fields of technology. ITO nanoparticles have played a vital role in photo-electronic devices, photovoltaic cells, electro-chromic devices (Devi et al. 2002), liquid crystal displays, plasma displays, heat reflecting mirrors, sensor modules (Yu et al. 2003), solar cells and electro-luminescent devices (Okuya et al. 2007), electrodes (Jo et al. 2011), telecommunication (Meng and Placido 2003), photo-catalysis (Yumoto et al. 1999), electromagnetic shielding, functional glass (Giusti 2011) and Laser Patterning (Risch and Hellmann 2011).

Indium tin oxide (ITO) behaves as an insulator in its stoichiometric form but it becomes a highly conductive semiconductor with a wide direct band gap (Eg = 3.6 eV)

[1), 2)] Professor

in its non-stoichiometric form. Hence it can be utilized in both forms, according to the desired properties (Li et al. 2006). Indium oxide crystallizes in two types; rhombohedral and cubic structure. Cubic is also known as bixbyite structure. This structure is related to that of fluorite structure if one fourth of the anions are removed and small shifts of the ions are allowed. Indium cations take the positions of two non-equivalent six-fold equipoints 'b' and 'd'. B-site cations are bounded by two structural body-diagonal vacancies and d-site cations are bounded by two structural face-diagonal vacancies. It should be kept in mind that these structural vacancies are in fact vacant oxygen interstitial positions (Mason et al. 2002).

Lower dimensional ITO nano-particles have got an enormous attention of the researchers. At present, nano-particles, nanometer spheres, nano-wires, nano-rods and nano-tubes have been prepared by variety of techniques (Bin et al. 2009, Yu et al. 2003). Generally, indium oxide and tin oxide powders are mixed together and compacted by hot or cold isostatic pressing as well as by sintering (Kolawa et al. 1998) ITO films, ITO coatings (Devi et al. 2002), electronic nano-devices (Yu et al. 2003) and nano-crystals have large scale applications in the modern times (Yumoto et al. 1999). Different techniques like co-precipitation, vapor-liquid-solid (VLS), sol-gel combustion, hydrothermal, spray combustion, micro-emulsion (Bin et al. 2009) evaporation, sputtering, chemical vapour deposition (Devi et al. 2002), electron vaporation, DC and rf magnetron sputtering, reactive thermal deposition, laser ablation (Yu et al. 2003) and microwave heating methods have been developed successfully (Okuya et al. 2007). Among all these methods, sol–gel method is very important one in order to obtain the desired properties of the ITO nano-particles [38]. For the deposition of ITO as anti-reflecting coating, usually thickness of 750 Å was required and if it deposited as high conductivity coating then several thousand thick layer is required. Conductivity of front layer is increased by using it in typical pn-junction silicon solar cell (Mason et al. 2002).

Sol-gel synthesis has many advantages over all of the above methods. It synthesis ultra-high pure materials (99.99%) at very low temperature of 150-600 °F. Almost every material can be synthesis and also co-synthesis of more than one material simultaneously. Coating of more than one material became easiest. Homogeneous composites and alloys produced through it. Microstructure, mechanical, physical and chemical properties of the resultant product can be explicitly restraint through it (Mason et al. 2002).

ITO films show maximum transmission, up to about 80-90% for the visible spectrum. This depends on the deposition conditions of the films. ITO films show high absorption in UV region and it's due to its band gap value which is 3.5eV. This absorption is directly associated with inter-band transitions. The band gap of ITO films lies in between 3.5-4.1eV. Wide optical band gap (> 3.5 eV) tries to minimize inter-band transitions due to which this transmission occurs (Giusti 2011)

In this research work, we have investigated the structural, optical and electrical properties of tin oxide and indium doped tin oxide thin films, synthesized by using sol-gel method for their applications in photovoltaic.

2. EXPERIMENTAL DETAILS

Sol-gel auto-combustion technique was used for the preparation of thin films of tin oxide (SnO_2) doped and un doped. For the preparation of compositions required proportion of the Anhydrous indium chloride ($InCl_3$) and anhydrous tin chloride ($SnCl_4$) were measured with the help of a precise digital balance. All the materials were in powder form. Anhydrous indium chloride ($InCl_3$) and anhydrous tin chloride ($SnCl_4$) were dissolved in ethanol (C_2H_5OH) separately, and then mixed to make a total volume of 50 ml. pH-meter measured the pH of the solution as 2.5 and a few drops of acetic acid (CH_3COOH) was added in indium oxide sol as complexing agent.

The magnetic stirrer was put in the solution and beaker was placed on a hotplate. Stirring of solution was started and temperature of the hotplate was increased gradually up to 150 ^oC. The solution was heated and stirred for about 45 minutes, till the gel was formed. As the gel was formed, the temperature of the sample was further decreased. The gel was cooled down and thin films were deposited on glass substrate.

After complete deposition of the thin films, the samples were placed in furnace for annealing. Thin films were annealed at different temperature. Two samples were prepared at two different temperatures. First both tin oxide doped and un doped In_2O_3 thin films were annealed at 50 ^oC to 500 ^oC. After removing from furnace, the samples were cooled down at room temperature. Structural properties of the prepared thin films were studied after characterization by X-Ray Diffrectometer. Bruker D8-Adverance diffractometer (Cu Kα radiation (λ = 1.54060 Å) in the Bragg'V GLIUDFWLRQ DQJOH µ ¶ ranging from 20 to 80 was used to study structural properties. Diffraction angle was adjusted from 30° to 80° with step width of 0.02°. Optical properties of the ZnO thin films were studied by J.A. Wollam spectroscopic ellipsometer to calculate band gap, wavelength and refractive index. The resistivity of thin films was calculated by using Four-point probe method.

3. RESULTS AND DISCUSSION

Fig. 1 shows XRD patterns of In_2O_3 at the temperature of 300 °C**.** The presence of various phases and grain size is determined from x-ray diffraction pattern.

XRD plot of In2O3 confirms the crystalline structure of the material. The diffraction peaks at around 30.05°, 33.1°, 35.1°, 40°, 41.2°, 41.6°, 44.6°, 46.7°, 48.5°, 53.7°, 54.8° are assigned to In_2O_3 (222), (321), (400), (420), (332), (332), (422), (431), (521), (433) and (600) respectively. All the peaks are well consisted with JCPDS card no. 6-0461 which confirms the cubic bixbyite structure with the average crystallite size of 37 nm and lattice parameter a= 10.25 Å which is in good agreement with Ghimbeu et al. (2008).

Fig. 2 shows the XRD pattern of SnO_2 thin film annealed at 300 ^oC which confirms the orthorhombic structure. All the peaks are matched with JCPDS card no. 29-1484. The average crystallite size was 30 nm.

Crystalline size of different samples is calculated by using Debye Scherrer formula which is given in Eq. (1) (Cullity 1978).

$$D = \frac{0.9\lambda}{\beta \cos\theta} \qquad (1)$$

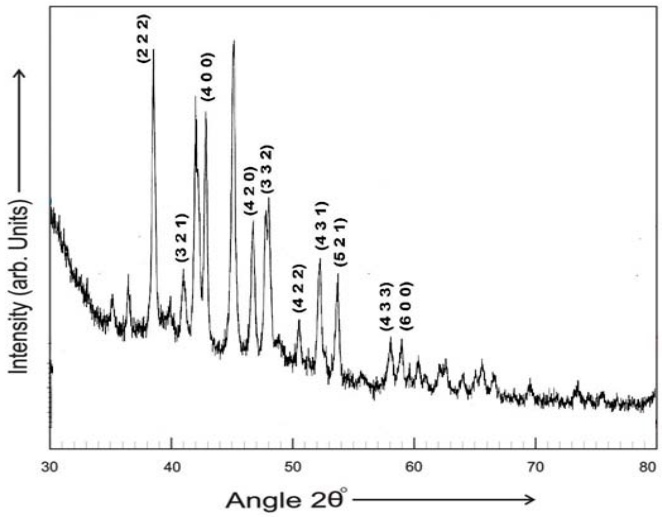

Fig. 1 XRD pattern of In_2O_3 synthesized at 300 ^oC

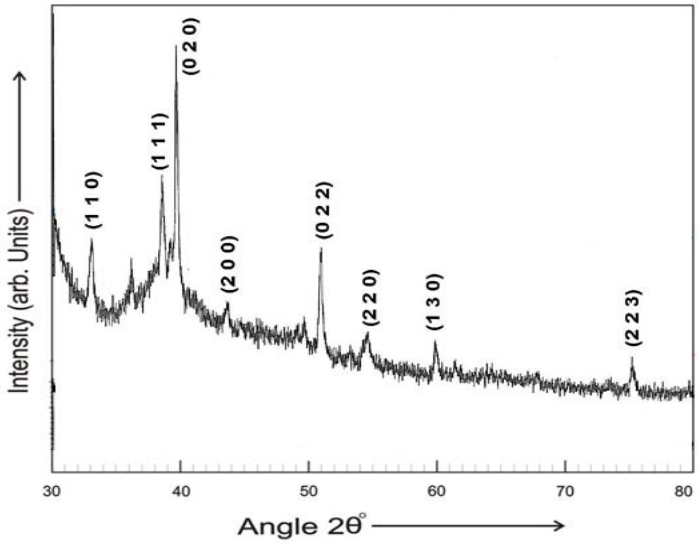

Fig. 2 XRD pattern of SnO_2 synthesized at 300^oC

Where, D, B, λ and θ are crystalline grain size, FWHM of the observed peak, wavelength of the x-ray diffraction and angle of diffraction, respectively. From the XRD pattern peak broadening is observed. With the decrease in FWHM, there is an increase in the crystallite size. Different samples of SnO_2 doped In_2O_3 thin films were prepared by spin coating and then annealed at the temperature range of 50^oC to 500^oC. Four of the samples were characterized by XRD analysis**.** Fig. 3 (a-d) shows XRD results of ITO thin films annealed at 50^oC, 100^oC, 400^oC and 500^oC. The matching of standard values with calculated values shows the hkl values for different lines on the pattern. The characteristics peak of S1 observed at an angle of 30.3^o assigned to $(12\ \bar{1})$, 38.6^o assigned to (220), 50.5^o assigned to $(12\ \bar{4})$ and 70^o assigned to (045) positions

respectively. This confirms the rhombohedral structure according to JCPDS card no. 88-0773. As temperature increases from 100^{o}C to 500^{o}C, their structure remains rhombohedral.

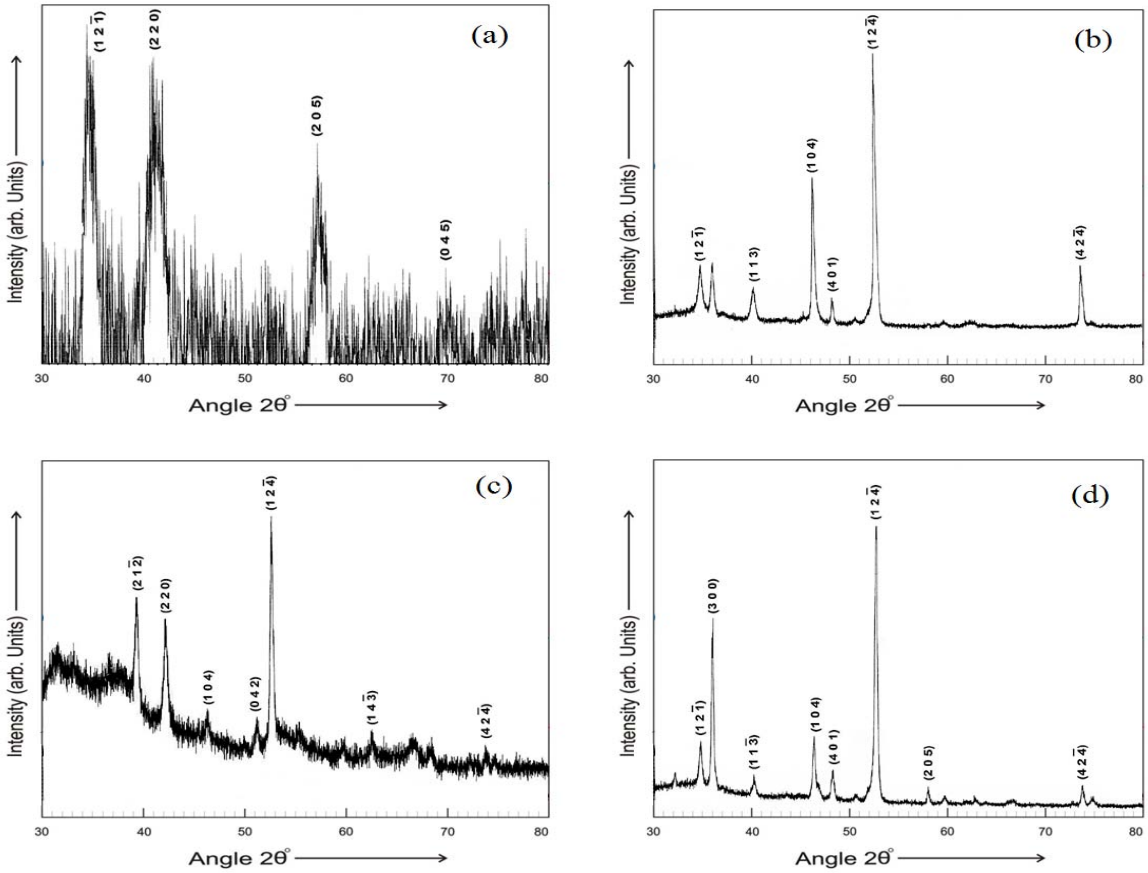

Fig. 3 XRD Pattern of ITO thin film annealed at a) 50^{o}C, b)100^{o}C, c) 400^{o}C, and d) 500^{o}C

In Fig. 3 (a) The characteristic peaks of ITO thin films annealed at 50^{o}C observed near 30^{o} at (12$\bar{1}$), 43^{o} at (104), 50^{o} at (12$\bar{4}$) and 74^{o} at (42 $\bar{4}$)) positions. Which are closely matched with JCPDS card 88-0733 (Mohammadi et al. 2013). Processing parameters plays key role in the structure and orientation of polycrystalline thin films. Recovery takes place when a metal or alloy annealed at low temperature and recrystallization occurs at high temperature. Recovery changes certain properties without any change in microstructure while recrystallization has some distinguishable structural changes with new grains. Since stress is the dominant cause of peak broadening, it has been observed that broad diffraction lines are partially sharpen during recovery but during recrystallization the lines attains their maximum sharpness. When a metal is recrystallized by annealing, the new grain structure must have a preferred orientation which is usually different from the metal of cold-work or annealed at low temperature. This is referred as annealing texture or crystallization texture

(Cullity 1978). The preferred orientation shows along the direction of (1 2 $\bar{1}$) for thin film of ITO annealed at 50°C. Temperature increased from 100°C to 500°C so the preferred orientation of the samples shifted from (12 $\bar{1}$) to (12$\bar{4}$).

The average crystallite size was calculated by FWHM of the most intense diffraction peaks in the XRD patterns. From the Fig. 4 it can be observed that crystallite size is 10.9 nm at 50°C. As the temperature increases upto 100°C, the crystallite size increases to 17.5 nm further increase in temperature, the crystallite size also increases. At 400°C and 500°C the observed crystallite size is 21.9 nm and 29.3 nm respectively. The crystallite size of 20 nm at 550°C have been reported in previous research (Li et al. 2008).

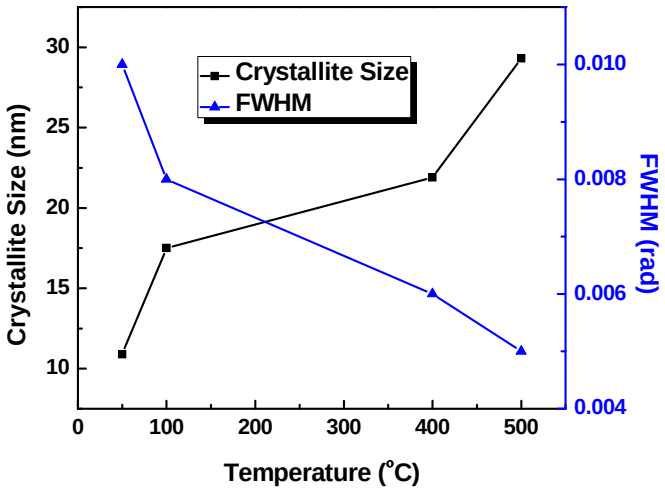

Fig. 4 Effect of temperature on crystallite size and FWHM

Lattice parameter for rhombohedral structure can be calculated from Eq. (2) for all the samples (Cullity 1978).

$$\frac{1}{d^2} = \frac{\left(h^2+k^2+l^2\right)\sin^2\alpha + 2\left(hk+kl+hl\right)\left(\cos^2\alpha - \cos\alpha\right)}{a^2\left(1-3\cos^2\alpha+2\cos^3\alpha\right)} \qquad (2)$$

Here “d” is d-spacing, hkl are Miller indices and “a” is the lattice parameter. In case of rhombohedral structure all the lattice parameters are equal i.e. a=b=c. The volume of the unit cell can be calculated from the above values by using Eq. (3) for rhombohedral structure.

$$V = a^3\sqrt{\left(1-3\cos^2\alpha+2\cos^3\alpha\right)} \qquad (3)$$

The value of lattice parameter goes decreasing by increasing the annealing temperature. This is due to the decrease in broadening of the peaks. As lattice parameter a decreased by increasing temperature, the volume also decreased Fig. 5 shows variation of lattice parameter with temperature.

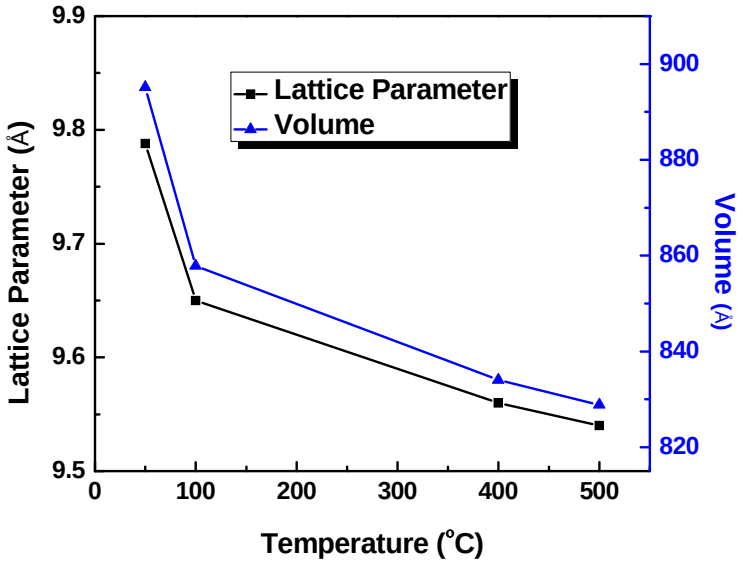

Fig. 5 Effect of temperature on lattice parameters

Dislocation density is calculated by the crystallite size “D”. It expresses the extent of defects in crystal (Mahmood et al. 2013). Its relation is given as

$$\rho = \frac{1}{D^2} \qquad (4)$$

From the relation it is clear that dislocation density decreased with the increase in crystallite size. So the presence of defects become minimum Fig. 6 shows the graph of dislocation density.

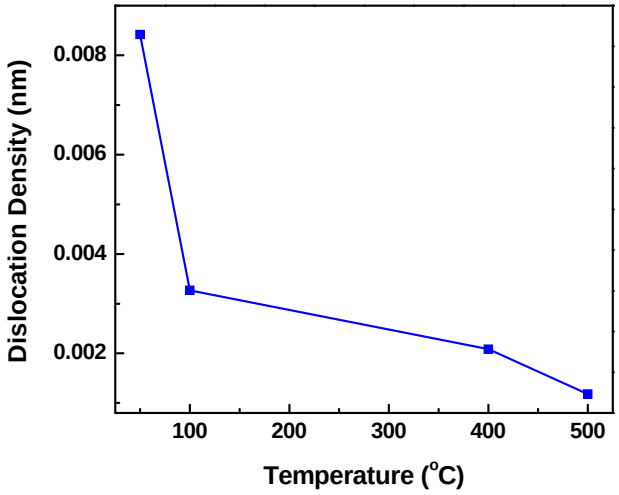

Figure 4.6: Effect of temperature on dislocation density

Crystallite size (D), lattice parameter (a), volume (v), strain and dislocation density (ρ) for ITO thin films annealed at temperature of 50°C, 100°C, 400°C and 500°C respectively are mention in table. 1.

Table 1: Calculated values of lattice parameter, volume of unit cell, strain and dislocation density for various ITO thin films

Parameters/Temperature	***50 ℃***	***100 ℃***	***400 ℃***	***500 ℃***
D (nm)	10.9	17.5	21.9	29.3
Lattice Parameter (Å)	9.78	9.65	9.56	9.54
Unit Volume ($Å^3$)	895.17	857.83	834.05	828.83
Strain	0.0093	0.0079	0.0015	0.0011
Dislocation Density ($X10^{-3}$ nm^{-2})	8.42	3.26	2.08	1.18

All the parameters decreased by increasing the annealing temperature of the thin films except crystallite size. when crystallite size increases, broadening decreased as both are reciprocal to each other. When there will be a decrease in broadening, strain also decreased. Decrease in strain also responsible for the decrease in lattice parameter and volume. Dislocation densities also have inverse proportion with crystallite size.

Variable angle spectroscopic ellipsometry was used for the optical characterization of ITO thin film. The material which is going to be used in optical applications or solar cell must have high transmission in the visible region of spectrum (400-700 nm) the Fig. 7shows the relation between wavelength and transmittance

results for all the six samples of ITO annealed at 50^{o}C, 100^{o}C, 200^{o}C, 300^{o}C, 400^{o}C and 500^{o}C.

The results show that all the samples have high transmittance for visible to infrared portion of the spectrum. The transmission have a sudden increase at 350 nm to 370 nm and reaches to 90% and then have slight increase in the infrared region which is different for all the six samples. Thin film annealed at 50^{o}C shows the highest transmission while the film annealed at 500^{o}C shows less transmission of 80% as compared to others as the transmission decreased gradually by increasing the temperature because of free carrier absorption. ITO annealed at 50^{o}C, 100^{o}C, 200^{o}C, 300^{o}C, 400^{o}C shows the maximum transmission of about 90 % which is in good agreement with previous work (Beena et al. 2009).

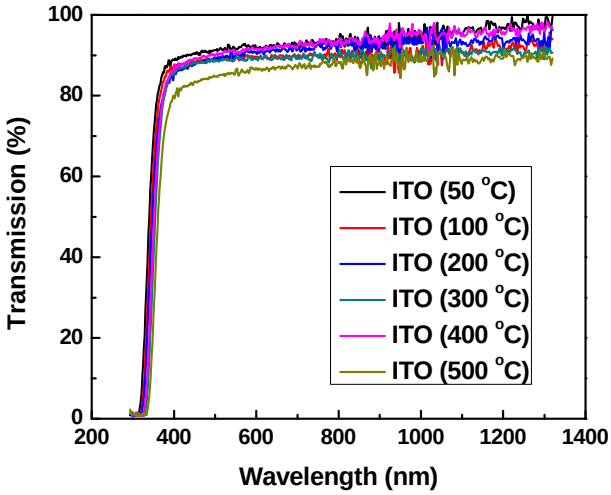

Fig. 7 Transmission of ITO thin films

Refractive index is an important optical parameter which gives the measure of transparency of material. After calculating extinction coefficient, the values of refractive indices for ITO thin films annealed at 50 ^{o}C, 100 ^{o}C, 200 ^{o}C, 300 ^{o}C, 400 ^{o}C and 500 ^{o}C estimated. Fig. 8 shows the relation between extinction coefficient and wavelengths of all the samples. Value of extinction co-efficient decreased by increasing the wavelength. ITO annealed at 500^{o}C has greater value of extinction coefficient because it has less transmission as compared to ITO annealed at 50^{o}C, 100 ^{o}C, 200^{o}C, 300 ^{o}C, 400^{o}C. Values of extinction coefficient have direct relation with the absorption of light in the medium. If transmissions have greater values than the values of absorption decreased and consequently the values of extinction coefficient also decreased. From the graph given below it is clear that the values of extinction coefficient decreased in the visible region by increasing the annealing temperature of ITO thin films which is related to the results of (Jung 2004).

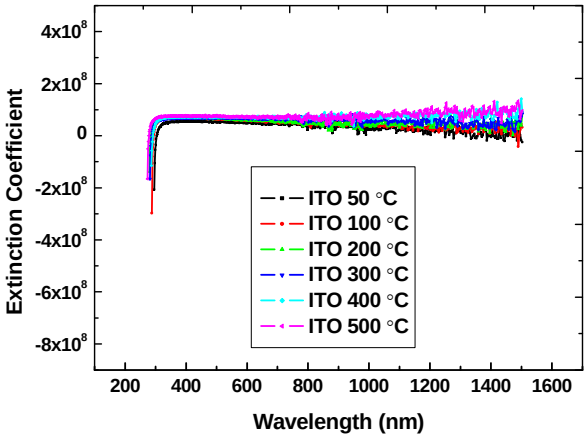

Fig. 8 Variation in extinction coefficient "*k*" of ITO thin films

After calculating extinction coefficient the values of refractive index "n" of all the samples were calculated. ITO is commonly used in optoelectronic devices and the refractive index of ITO plays an important role in the optical properties because it has great contribution in different optical conditions including diffraction, reflection, absorption and transmission (Jung 2004).

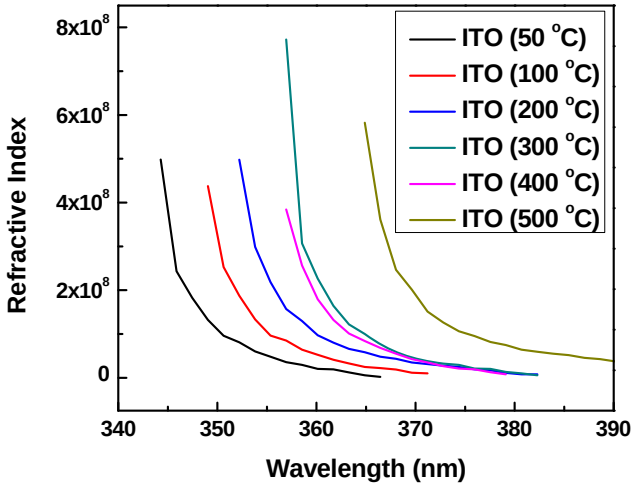

Fig. 9 Variation in refractive index "n" of ITO Thin Films

Fig. 9 shows the refractive indices of the samples. Refractive index also decreased by increasing the wavelength.The extinction coefficient and refractive index decreased by increasing the wavelength. The decreases in extinction coefficient and refractive index have a relation with the increase in transmission. The decrease in the value of extinction coefficient with increase in wavelength shows the extent of transmission of light reduced by absorption or dispersion. The decrease in the value of refractive index by increasing wavelength indicates normal dispersion of light.

The ellipsometry results for band gap are given in Fig. 10 (a-f**).** The plots of energy versus α^2 (absorption coefficient) have a linear region which correspond the electron excitation from valance to conduction band and incident energy of photon. Fig. 10 (a**)** shows the band gap of ITO thin film annealed at 50^{o}C.

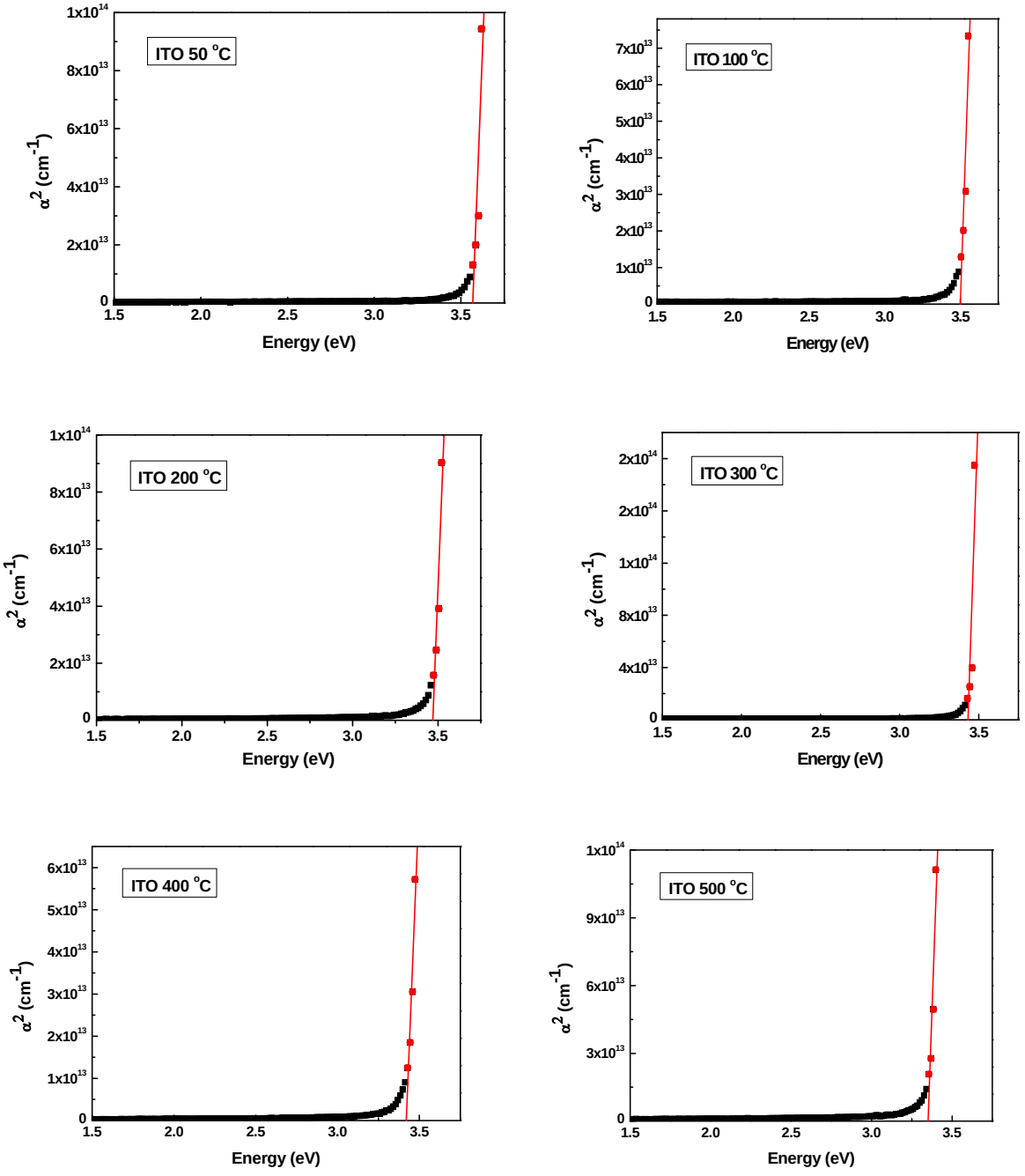

Fig. 10 Band gap of ITO thin film at a) 50 ^{o}C, b) 100 ^{o}C, c) 200 ^{o}C, d) 300 ^{o}C, e) 400 ^{o}C and f) 500 ^{o}C

ITO thin films annealed at 50^{o}C, 100^{o}C, 200^{o}C, 300^{o}C, 400^{o}C and 500^{o}C have band gap of 3.5 eV, 3.49 eV, 3.44 eV, 3.43 eV, 3.42 eV, 3.36 eV, respectively. Fig. 10 (b) shows the band gap of ITO thin film annealed at 100 ^{o}C. Fig. 10 (c) shows the band gap of ITO thin film annealed at 200^{o}C. Fig. 10 (d) shows the band gap of ITO thin film annealed at 300^{o}C. Fig. 10 (e) shows the band gap of ITO thin film annealed at 400^{o}C. Fig. 10 (f) shows the band gap of ITO thin film annealed at 500^{o}C. When annealing temperature increased, the carrier concentration increased in the sample because of the increased mobility of electron-hole pairs. In the case of ITO, the carrier concentration increased by Sn doping. So when these samples annealed their band gap also changed due to the mobility of charge carriers (Fallah et al. 2010).

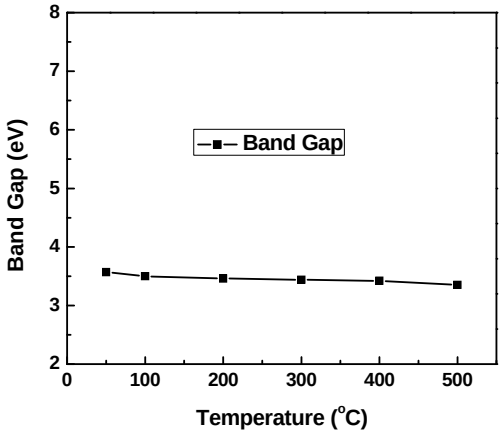

Fig. 11 Effect of temperature on band gap

In this case the highest value of band gap has been obtained at 50^{o}C that is 3.5 eV. Fig. 11 shows band gap with the change in temperature.

4. CONCLUSIONS

The influence of temperature on structural, optical and electrical properties of ITO thin films was studied. From the obtained graph form XRD, it is confirmed that our sample grew with the orientation of $(12\bar{1})$, (104), $(12\bar{4})$ and $(42\bar{4})$ that prove the rhombohedral structure of ITO. The calculated value of crystallite size was 10.9 nm at 50^{o}C than increased constantly with the increasing temperature. The crystallite size for 100^{o}C, 400^{o}C and 500^{o}C was 17.5 nm, 21.9 nm, 29.3 nm respectively. The lattice parameter was calculated as an average of 9.6 Å. The results of XRD show that temperature affects the crystallite size of ITO thin films. Spectroscopic ellipsometry was used to characterize the optical properties of thin films. The results reveal the transmission, absorption c0efficient, refractive index and band gap of all the samples. ITO thin films have high transmission of 85%. Band gap of the thin films were determined which is 3.36eV to 3.53eV. So it is favorable for optoelectronic devices and solar cells applications. The electrical properties were also analyzed.

REFERENCES

Beena, D., Lethy, K.J., Vinodkumar, R., Pillai, V.P.M., Ganesan, V., Phase, D.M. and Sudheer, S.K. (2009), "Effect of substrate temperature on structural, optical and electrical properties of pulsed laser ablated nanostructured indium oxide films," *Appl. Surf. Sci.,* **255**(20), 8334-8342.

Bin, Z.X., Tao, J., Zhou, Q.G. and Yun, H.B. (2009), "ITO nano-powders prepared by microwave-assisted co-precipitation in aqueous phase," *T. Nonferr. Metal. Soc.,* **19**, S752-S756.

Cullity, B.D. (1978), "Elements of X-Ray Diffraction", 2nd Ed., Addison-Wesley Publishing Company, Inc.

Devi, P.S., Chatterjee, M. and Ganguli, D. (2002), "Indium tin oxide nano-particles through an emulsion technique," *Mater. Lett.,* **55**, 205–210.

Fallah, H.R. Varnamkhasti, M.G. and Vahid, M.J. (2010), "Substrate temperature effect on transparent heat reflecting nanocrystalline ITO films prepared by electron beam evaporation," *Renewable Energy* **35**(7), 1527-1530.

Ghimbeu, C.M., Schoonman, J. and Lumbreras, M. (2008), "Porous indium oxide thin films deposited by electrostatic spray deposition technique," *Ceram. Inter.,* **34**(1), 95-100.

Giusti, G. (2011), "Deposition and Characterisation of Functional ITO Thin Films", School of Metallurgy and Materials, The University of Birmingham, Birmingham, PhD thesis.

Jo, Y.J., Hong, C.H. and Kwak, J.S. (2011), "Improved electrical and optical properties of ITO thin films by using electron beam irradiation and their application to UV-LED as highly transparent p-type electrodes," *Cur. Appl. Phys.,* **11**, S143–S146.

Jung, Y.S. (2004), "Spectroscopic ellipsometry studies on the optical constants of indium tin oxide films deposited under various sputtering conditions," *Thin Solid Films*, **467**, 36-42.

Kolawa, E., Garland, C., Tran, L., Nieh, C.W., Molarius, J.M., Flick, W., Nicolet, M.A. and Wei, J. (1988), "Indium oxide diffusion barriers for Al/Si metallizations," *Appl. Phys. Lett.,* **53**, 2644-2649.

Li, S., Qiao, X., Chena, J., Wang, H., Jia, F. and Qiu, X. (2006), "Effects of temperature on indium tin oxide particles synthesized by co-precipitation," *J. Crys. Growth,* **289**, 151–156.

Li, Z., Ke, Y. and Ren, D. (2008), "Effects of heat treatment on morphological, optical and electrical properties of ITO films by sol-gel technique," *T. Nonferr. Metal. Soc.,* **18**(2), 366-371.

Mason, T.O., Gonzalez, G.B., Kammler, D.R., Hadavi, N.M. and Ingram, B.J. (2002), "Defect chemistry and physical properties of transparent conducting oxides in the CdO-InO-SnO system," *Thin Solid Films,* **411**, 106–114.

Mehmood, W., Shah, N.A., Akram, S., Mehboob, U., Malik, U.S. and Sharaf, M.U. (2013), "Investigation of substrate temperature effects on physical properties of ZnTe thin films by close spaced sublimation technique," *Chalcogenide Letters,* **10**(8), 273-281.

Meng, L. and Placido, F. (2003), "Annealing effect on ITO thin films prepared by microwave-enhanced dc reactive magnetron sputtering for telecommunication applications," *Sur. Coat. Techn.,* **166** 44–50.

Mohammadi, S., Abdizadeh, H. and Golobostanfard, M.R. (2013), "Effect of niobium doping on opto-electronic properties of sol–gel based nanostructured indium tin oxide thin films," *Ceram. Inter.,* **39**(4), 4391-4398.

Okuya, M., Ito, N. and Shiozaki, K. (2007), "ITO thin films prepared by a microwave heating," *Thin Solid Films*, **515**, 8656–8659.

Risch, A. and Hellmann, R. (2011), "Picosecond laser patterning of ITO thin films," *Phys. Proc.,* **12**, 133–140.

Yang, L.L., He, X.D., He, F. and Sun, Y. (2009), "Small angle X-ray scattering studies on structural evolution during calcination of sol–gel ITO nano-powders," *J. Alloy. Compd.,* **470**, (2009) 317–322.

Yu, D., Wang, D. Yu, W. and Qian, Y. (2003), "Synthesis of ITO nanowires and nanorods with corundum structure by a co-precipitation-anneal method," *Mater, Lett.,* **58**, 84–87.

Yumoto, H., Inoue, T., Lia, S.J., Sakoa, T. and Nishiyama, K. (1999), "Application of ITO films to photocatalysis," *Thin Solid Films,* **345**, 38-41.